First Performance of the GeMS+GMOS system.

Pascale Hibon[a], Benoit Neichel[b], Vincent Garrel[a], Benjamin Prout[c], Francois Rigaut[c], Alice Koning[d], Gaetano Sivo [a], German Gimeno[a], Rodrigo Carrasco[a], Claudia Winge[a], Peter Pessev[a], Andrew Serio[a], Gustavo Arriagada[a]
[a]Gemini South Observatory, Casilla 603, La Serena, Chile
[b] Laboratoire d'Astrophysique de Marseille, Technopole de Chateau-Gombert, Marseille, France
[c] Australian National University, Barry Dr Acton Australian Capital Territory 0200, Australia
[d] University of Victoria, 3800 Finnerty Rd Victoria, BC V8P 5C2, Canada

ABSTRACT

During the 2012 commissioning of the Gemini MCAO System (GeMS) in Gemini South Observatory, we briefly explored the performance improvement brought by pairing GeMS with the Gemini Multi-Object Spectrograph (GMOS), compared to GMOS in natural seeing mode. GMOS is an instrument sensitive in the visible band with imaging and spectroscopic capabilities, hence pushing MCAO toward the visible, a mode for which it was not specifically designed.
We report in this paper the first results obtained with the GeMS +GMOS pair. Several globular clusters were observed in imaging mode only. We have derived performance in term of FWHM and determined the improvement against natural seeing. We also obtain photometric, relative and absolute astrometric precision for the AO enhanced images. We also studied the influence of the NGS constellation on the photometric performance.
Finally, we also looked at the expected performance of the GeMS+GMOS system once the CCD upgrade, scheduled during 2014, will occur.

Keywords: adaptive optics, instrumentation, visible

1. INTRODUCTION

1.1 GMOS: Gemini Multi-Object Spectrograph

The GMOS spectrograph is capable of both long-slit and multi-slit spectroscopy, is equipped with integral field units (IFU), in addition to an imaging mode with a 5.5' x 5.5' field of view over three CCD chips with a pixel scale of 79 mas, values when we are in seeing-limited conditions (see Table 1). The three CCD chips form a 6144 x 4608 pixel array, with two gaps of about 37 pixels separating the detectors.[1] In its imaging mode, GMOS-S has six standard broad band filters: u-band (336-385nm), g-band (398-552nm), r-band (562-698nm), i-band (706-850nm), CaT-band (780-933nm) and z-band (848-1000nm). The present paper focus on GMOS-S's imaging capabilities.

1.2 GeMS: Gemini Multi-Conjugate Adaptive Optics System

First of its kind, GeMS is a laser assisted Multi Conjugate Adaptive Optics System.[2] It, uses five sodium laser guide stars, four at each corner of a 60" square and one in the centre to form an X-shaped constellation. In order to measure tip-tilt orders, it can use up to 3 natural guide stars in a 2' patrol field. GeMS currently uses 2 deformable mirrors (one missing from the design) and a TT mirror to produce close to diffraction limit performance in the near infrared bands.[3] In order to better understand its scientific capabilities and to provide more thorough documentation for future users of this system, we aim to create image quality maps based on full-width half-maximum (FWHM) measurements and to determine the throughput of the GeMS+GMOS system by comparing it to the known throughput of GMOS alone.

Address all correspondence to: Pascale Hibon, Gemini South Observatory, Casilla 603, La Serena, Chile, Tel: +56 512-205-680; E-mail: phibon@gemini.edu

Ground-based and Airborne Instrumentation for Astronomy V, edited by Suzanne K. Ramsay, Ian S. McLean, Hideki Takami, Proc. of SPIE Vol. 9147, 91478T · © 2014 SPIE · CCC code: 0277-786X/14/$18 · doi: 10.1117/12.2055196

1.3 GeMS+GMOS system

During the commissioning of the Gemini MCAO System (GeMS), we had the opportunity to obtain data with the Gemini Multi-Object Spectrograph (GMOS) in March and May 2012. Due to the change of focal-ratio, the FoV is now, the imaging field of view is now 2.5 x 2.5 arcmin2, the pixel scale is 35.9 mas and the only filters available are the i-band (706-850nm), CaT-band (780-933nm) and z-band (848-1000nm). We observed 14 globular clusters with the GeMS+GMOS system between these two periods. Table 1 summarized the differences when using GMOS and the system GeMS+GMOS.

Table 1. Table comparing the specificities of GMOS and GeMS+GMOS.

System	f/D	Field of View	Pixel Scale	Available Broad Band Filters
GMOS	16	5.5' x 5.5'	79 mas	u, g, r, i, CaT, z
GeMS+GMOS	33	2.5' x 2.5'	35.9 mas	i, CaT, z

2. FWHM PERFORMANCE

The star detection and the FWHM values are obtained by running SExtractor[4] on the reduced images. Figures 1, 2, 3, and Table 2 present the field images with the Natural Guide Star (NGS) Constellation and the studied area, for which the FWHM has been determined, and the FWHM maps for four different globular clusters observed in i- or z-band.

Table 2. Table of the performance of the GeMS+GMOS system.

NGC	Observed Band	Exp. Time	Natural Seeing	Average FWHM	Abs. Astrometric Error
NGC 4590	i-band	5 sec	0.8"-1.1"	382.6 mas	3.04 mas
NGC 6496	i-band	5 sec	0.8"-1.1"	635.5 mas	5.39 mas
NGC 5286	z-band	5 sec	0.7"	335.6 mas	4.4 mas

We remarked that for these four fields, we obtained an improvement factor between the natural seeing and the FWHM obtained in the images in the range of 1.6 to 2.8. From Table 2, we can also observed that for a same natural seeing range, the FWHM performance for NGC4590 and NGC6496 are almost a factor two apart.

This difference of performance, while the seeing was similar during the observations, can be explained by several reasons :

- the NGS constellations used were different.
- the laser return due to seasonal effects in the sodium layer. With less photons, the frequency of the loops has to be reduced in order to keep a sufficient SNR on the wavefront sensors. The temporal error grows accordingly and therefore the overall performance decrease.
- the turbulence profile: As GeMS is missing one of its DM conjugated at 4.5km, mid-altitude turbulence goes uncorrected. If the turbulence is strong, the anisoplanatism error grows and the overall performance decrease.[5]

Figure 4 shows the evolution of total and free-atmosphere seeing measured by the DIMM and MASS site monitor at Cerro Tololo on two nights. These measurements are a good approximation of the atmospheric conditions at Cerro Pachon as these two telescope sites are separated by 14km and have a 300m altitude difference. We can see in Figure 4 a., the MASS data are higher than the FWHM performance: the MCAO and the two Deformable Mirrors (DMs) have been correcting better than one DM could have done alone. However, Figure 4 b., the FWHM results are mostly located between the DIMM and MASS data. We are then correcting from the ground-layer turbulences, like a GLAO system would do. The main turbulence factor was then coming from another layer or GeMS performance were not optimal.

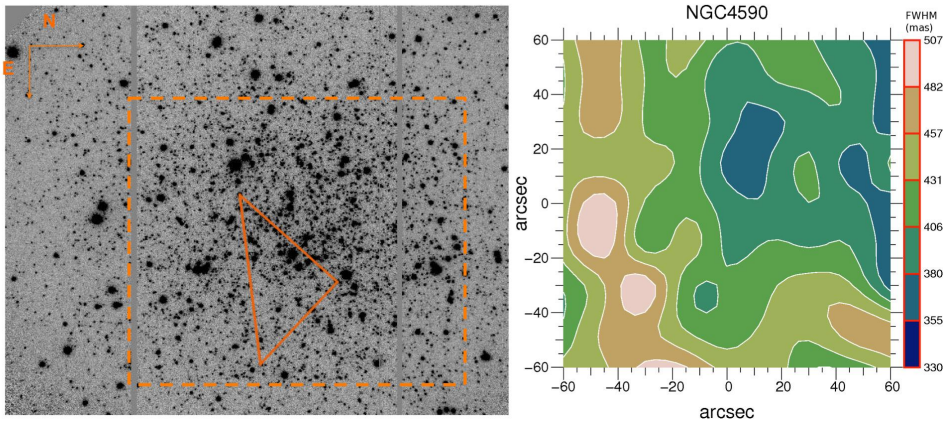

Figure 1. Left: Field image of NGC 4590 with the N-E orientation, the NGS constellation and the studied area marked. Right: FWHM map.

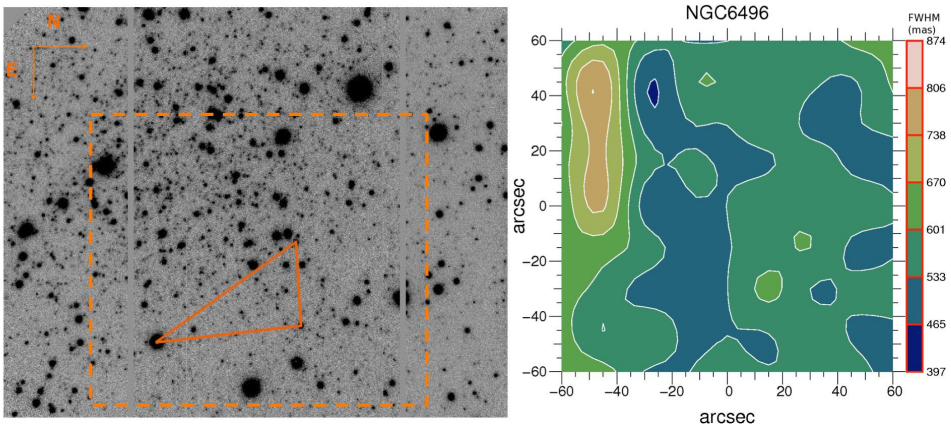

Figure 2. Left: Field image of NGC 6496 with the N-E orientation, the NGS constellation and the studied area marked. Right: FWHM map.

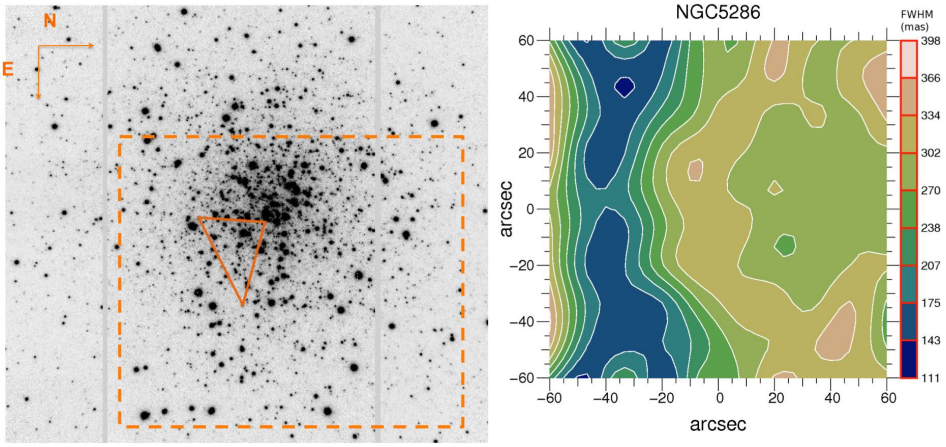

Figure 3. Left: Field image of NGC 5286 with the N-E orientation, the NGS constellation and the studied area marked. Right: FWHM map.

3. PHOTOMETRIC PERFORMANCE

3.1 Method

We expect the GeMS throughput to be lower than GMOS simply due to the added number of optical surfaces in the MCAO system, each of which absorbs some of the transmitted light. What we aim to estimate is by

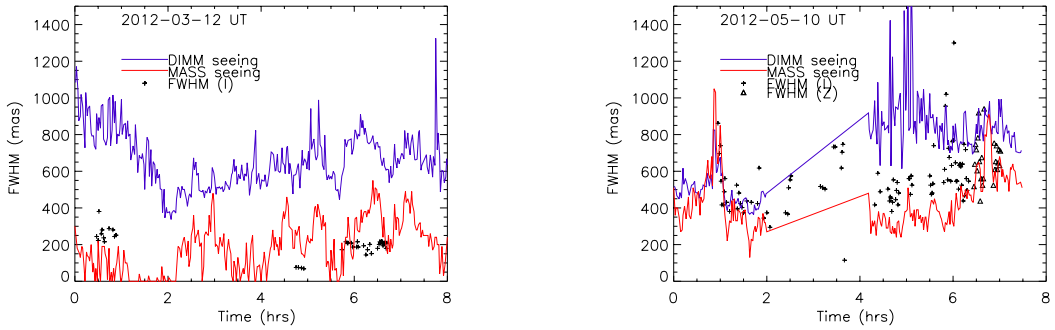

a. 2012-03-12 UT *b. 2012-05-10 UT*

Figure 4. Atmospheric conditions on two of the GeMS+GMOS nights. The blue lines show the total (DIMM) seeing, the red lines the free-atmosphere seeing (MASS). The crosses are the FWHM of i-band GeMS+GMOS images, the diamonds the FWHM of z-band GeMS+GMOS images. The errors on the FWHM is ± 20 mas.

how much the throughput deteriorates due to GeMS. We determined the difference of flux transmission between GMOS and the GeMS+GMOS system using the following equation (Eq. 1):

$$\text{GMOSGeMSThroughput} = \frac{\text{GMOSGeMSFlux}}{\text{GMOSFlux}} \times \frac{\text{GMOSExp.Time}}{\text{GMOSGeMSExp.Time}}. \quad (1)$$

To obtain an absolute value of this throughput difference, we only created maps for data that we have equivalent GMOS images in gain, filter and binning. Such data exist only in the i-band. In z-band, the throughput appears to be 10-20% less through GEMS compared to GMOS going straight onto the sky.

3.2 Results

Figure 5 shows the throughput difference in percentage for two globular clusters. Remarkably, for each individual frame, the GeMS throughput varies by less than 4.7% across the examined portion of the CCD chips.

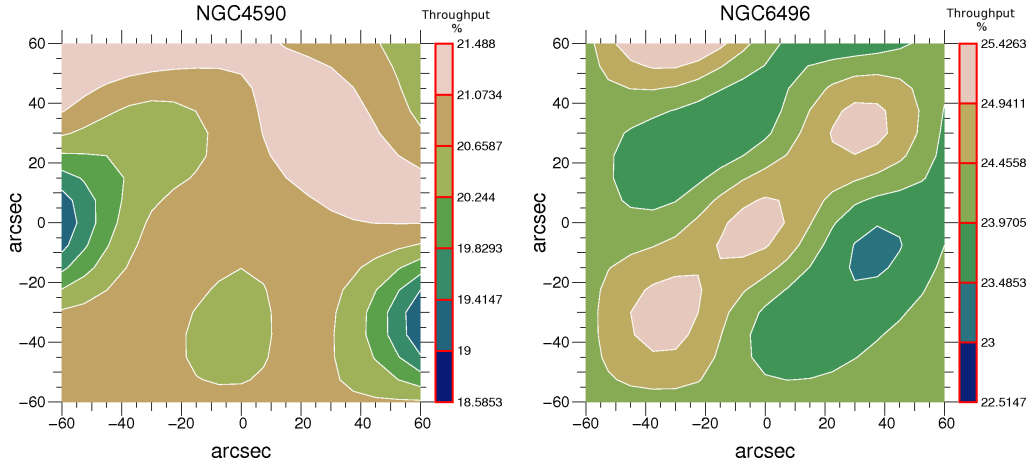

Figure 5. Throughput difference map in percentage for two globular clusters: NGC4590 (Left) and NGC6496 (Right).

The current Beam Splitter has a cutoff at 850nm while GeMS can for now close the loop on NGS stars of magnitude R∼15.5 (see Figure 6). We could replace it with a beam splitter with a cutoff at 600nm. This would

allow to observe with the r-band filter. However, this will impact the sky coverage. We estimate that we would roughly lose one magnitude from the current limiting magnitude. Another possibility will be to use a beam splitter sending only the laser light (λ=589nm) to the wavefront sensor and the rest to GMOS. In that case, the tip-tilt sensing would be done with a peripheral WFS on the telescope guiding system. This solution would allow observations with all the GMOS filters, however it would introduce more anisoplanatism in the images.

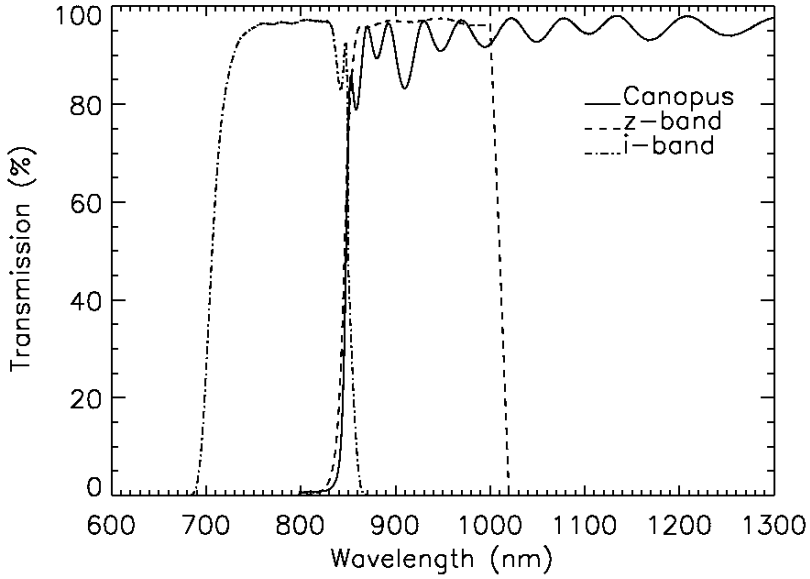

Figure 6. The solid line shows the Canopus transmission according to wavelength for the setup used in this work. The dashed line is the i-band filter transmission and the dot-dashed one the z-band filter transmission. It is evident that the beam-splitter cut-off point occurs within the i-band's 706-850nm range. This explains why the i-band throughput determined above is so much lower than we might expect from the GMOS throughput.

4. ASTROMETRIC PERFORMANCE

There are two different astrometry to take into account: the absolute astrometry and the relative astrometry.

4.1 Absolute astrometry

We are presenting here the case of NGC 4590. We have in our hands 31 individual images taken during the same night with the same configuration (exposure time, filter and binning). After founding the star position in each individual frame with SExtractor, we create a Master Reference Frame (MRF) from the average star position. We compared then the difference in position from all the individual images to the MRF. The results are shown in different ways: the astrometric error map (Figure 7 left), the comparision of the total astrometric error to the expected photon noise (Figure 7 center), and the frequency of the astrometric error (Figure 7 right). The photon noise is estimated following the equation Eq 2. For NGC4590, the average astrometric error is 3.04 mas.

$$\sigma_{photon} = \frac{\mathrm{FWHM}}{\sqrt{N_{\mathrm{photon}}}} \tag{2}$$

4.2 Relative astrometry

To measure the relative astrometry, we select one image from NGC4590, used for the absolute astrometry, and compare the distance from a central bright unsaturated star to the brightest (unsaturated) star in various regions of the sky. In the presented case, NGC4590, we chose nine different regions around the central star. From

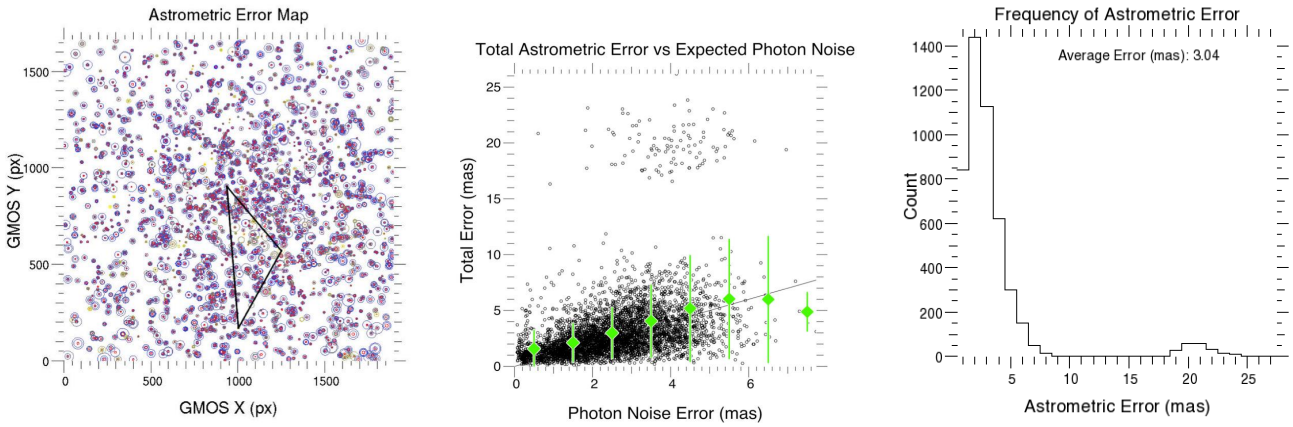

Figure 7. Left: Absolute astrometric error map. Each circle is centered on a star. Yellow circles are a high flux stars, blue circles are the low flux star. The red circles represente the estimated photon noise. Center: Astrometric error versus the expected photon noise. Right: Histogram showing the frequency of the astrometric error.

Figure 8, we show that we obtain a consistent precision for star to star distances lower than 50". When looking at the precision obtained over these nine regions, we remark that some regions are being better corrected from others. The mean separation values range from 13429 ± 2.3 mas to 45100 ± 6.6 mas. The best corrected regions are the ones located around the natural guide star constellation. This demonstrates then the importance of the NGS constellation choice and the discrepancy in performance depending on it.

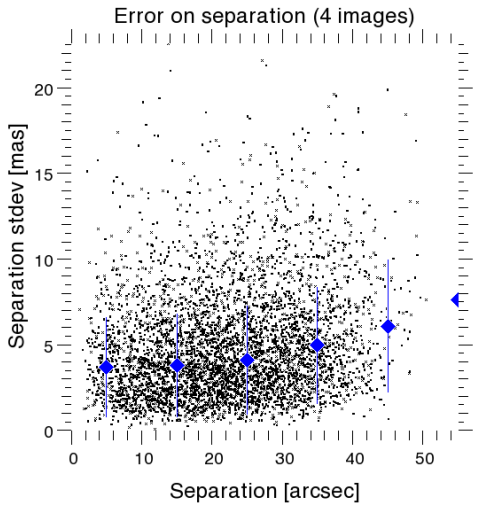

Figure 8. Star to star separation measurement. We obtain a consistent precision for star to star distances lower than 50".

5. DISCUSSION - CONCLUSION - QUICK PRESENTATION OF SCIENCE CASE

5.1 Science Case

The combination of the visible instrument GMOS with the MCAO system GeMS is a unique opportunity and could have an important scientific impact. Several astronomical areas could benefit of such a system. A detailed science case for the GeMS+GMOS system will be soon presented in Hibon et al. (in preparation).
The first and obvious application of such a system is the stellar clusters. We will be able to resolve stellar populations and obtain deeper magnitude limit from ground-based telescope. This will help with cluster classifications,

age, metallicity, distance and reddening determination.
Nebulae, and more specifically planetary nebulae, would also take advantage of this observing system in order to characterize their weak surrounding emissions and improve our understanding or their association with star formation.
Galaxies and the study of their morphology, their disk formation, their relation with the intergalactic medium (IGM), and the link between the evolution of the IGM and star formation, for examples, would too.
Moreover, faint targets, such as distant galaxies and gravitational arcs are also an important area to explore with visible MCAO. A large field of view with a great AO correction, and therefore a great improvement in resolution, is a great combination for studying the distant Universe.

5.2 Conclusion

We have in our hands the first MCAO visible data. The astrometric and photometric performance level reached is very encouraging to deepen the study and develop such a system. The complete sets of data and results obtained with the GeMS+GMOS combination and precise details on the analysis are presented in Hibon et al. 2014 (in preparation).
A CCD upgrade for GMOS-South is scheduled during the 2014A semester, which will increase its performances for the wavelength range [600-1050]nm. We are then expecting better performances of GeMS+GMOS. The GeMS+GMOS combination is also very interesting when used in Long-Slit and Multi-Object Spectroscopy mode. The gain in spatial resolution will not only allow us to use smaller slit size but it will also allow us to reduce the exposure time for a requested SNR, comparing to GMOS without AO. Thanks to GMOS versatility, we can also envisage the use of GeMS with the IFU mode (5"x7"), which will compete with the Narrow Field Mode (7.5"x7.5") of the system VLT/MUSE- GALACSI.

ACKNOWLEDGMENTS

Based on observations obtained at the Gemini Observatory, processed using the Gemini IRAF package, which is operated by the Association of Universities for Research in Astronomy, Inc., under a cooperative agreement with the NSF on behalf of the Gemini partnership: the National Science Foundation (United States), the National Research Council (Canada), CONICYT (Chile), the Australian Research Council (Australia), Ministério da Ciência, Tecnologia e Inovação (Brazil) and Ministerio de Ciencia, Tecnología e Innovación Productiva (Argentina).

REFERENCES

[1] I. M. Hook, I. Jørgensen, J. R. Allington-Smith, R. L. Davies, N. Metcalfe, R. G. Murowinski, and D. Crampton, "The Gemini-North Multi-Object Spectrograph: Performance in Imaging, Long-Slit, and Multi-Object Spectroscopic Modes," *PASP* **116**, 425–440 (2004).

[2] F. Rigaut, B. Neichel, M. Boccas, C. d'Orgeville, F. Vidal, M. A. van Dam, G. Arriagada, V. Fesquet, R. L. Galvez, G. Gausachs, C. Cavedoni, A. W. Ebbers, S. Karewicz, E. James, J. Lührs, V. Montes, G. Perez, W. N. Rambold, R. Rojas, S. Walker, M. Bec, G. Trancho, M. Sheehan, B. Irarrazaval, C. Boyer, B. L. Ellerbroek, R. Flicker, D. Gratadour, A. Garcia-Rissmann, and F. Daruich, "Gemini multiconjugate adaptive optics system review - I. Design, trade-offs and integration," *MNRAS* **437**, 2361–2375 (2014).

[3] B. Neichel, F. Rigaut, F. Vidal, M. A. van Dam, V. Garrel, E. R. Carrasco, P. Pessev, C. Winge, M. Boccas, C. d'Orgeville, G. Arriagada, A. Serio, V. Fesquet, W. N. Rambold, J. Lührs, C. Moreno, G. Gausachs, R. L. Galvez, V. Montes, T. B. Vucina, E. Marin, C. Urrutia, A. Lopez, S. J. Diggs, C. Marchant, A. W. Ebbers, C. Trujillo, M. Bec, G. Trancho, P. McGregor, P. J. Young, F. Colazo, and M. L. Edwards, "Gemini multiconjugate adaptive optics system review - II. Commissioning, operation and overall performance," *MNRAS* **440**, 1002–1019 (2014).

[4] E. Bertin and S. Arnouts, "SExtractor: Software for source extraction.," *Astronomy & Astrophysics Supplement* **117**, 393–404 (1996).

[5] M. Le Louarn, C. Verinaud, and V. Korkiakoski, "Simulation of MCAO on (extremely) large telescopes," *Comptes Rendus Physique* **6**, 1070–1080 (2005).

List of Figures

List of Tables